Thin-film anisotropic transport measurement on tilted $Bi_2Sr_2CaCu_2O_x$

J. S. Tsai, J. Fujita, and M. Yu. Kupriyanov*
NEC Fundamental Research Laboratories, 34 Miyukigaoka, Tsukuba 305, Japan
(Received 18 October 1994; revised manuscript received 10 February 1995)

To make a relevant transport measurement between adjacent Cu-O (or double Cu-O) layers, a high-quality single-crystal sample with a rather small area having a restricted number of Cu-O layers is required. To satisfy such requirements, we have prepared a tilted epitaxial $Bi_2Sr_2CaCu_2O_x$ film. The c axis of the film makes a nonzero angle with respect to the film normal. In a certain direction, the transport current has to traverse Bi-O layers. Few-micrometer-wide strips containing several tens of Cu-O layers in series were made. The resistivities, critical currents, and I-V characteristics showed marked anisotropies in two transport orientations. The possibility of direct observation of interlayer Josephson coupling was investigated. However, no ac or dc Josephosn effect was observed. The voltage near I_c seemed to be generated by the dynamics of the Josephson vortices. These observations are consistent with a theoretical analysis based on the Josephson-coupled layered model, which gives a Josephson penetration depth considerably smaller than our smallest sample size, and a transport analysis considering the detailed junction geometry.

I. INTRODUCTION

High-temperature superconductors containing Cu-O planes show strong anisotropy in magnetic as well as transport properties. For $YBa_2Cu_3O_{7-x}$, the anisotropy in H_{c2} precisely follows the prediction of the theory for Josephson-coupled two-dimensional layers and the anisotropic Ginzburg-Landau theory.[1] The anisotropy in resistivity above T_c for these materials is also very large: it is metal-like in the a-b direction and, for some materials, even semiconductive in the c direction, indicating the existence of different transport mechanisms in these two directions.[2] The obvious question is what kind of coupling mechanism for Cooper pair transfer is operating between the Cu-O planes below T_c. Is it truly Josephson coupling? The coherence length determined magnetically is surprisingly small in the c-axis direction; namely, about 0.1 nm or less for $YBa_2Cu_3O_{7-x}$ and $Bi_2Sr_2CaCu_2O_x$.[3] This is much smaller than the spacing between Cu-O planes in these crystals, suggesting the coupling is Josephson-like. The relatively longer Cu-O interlayer spacing in $Bi_2Sr_2CaCu_2O_x$ (about 12 nm) implies an even strong two dimensionality and weaker interlayer coupling than in $YBa_2Cu_3O_{7-x}$. Technologically speaking, such interlayer coupling might provide us a naturally formed high-quality high-T_c Josephson component which we might not be able to obtain otherwise.

For the transport measurement, indirect evidence of the existence of the Josephson interactions between the CuO planes was obtained in single-crystal break junctions.[4] These structures sometimes show the characteristics typical for superconductor-insulator-superconductor (SIS) or superconductor–normal-metal–superconductor (SNS) junctions (the shape of the I-V curve and usually a large I_cR_n product around 20–30 meV). Unfortunately, it was impossible not only to control the parameters of these structures but even to identify the physical locations of the junctions in the samples, so that the relation of these junctions to the intrinsic interlayer Josephson effect is still questionable. Subsequently, Kleiner *et al.*[5] reported the observation of the appearance of voltage steps on the I-V curve of single crystals under an applied microwave irradiation. The authors claimed that these steps were due to the intrinsic Josephson junctions naturally existing between CuO planes, working in a phase-locked mode of operation. However, the typical sizes of the samples $30\times30\times3$ μm^3 they used are larger than the effective radius of the Josephson vortices in the structure, $4\lambda_J \approx 4s\lambda_c/\lambda_{ab} \approx 0.5$ μm. In accordance with theoretical predictions,[6] in this experimental situation, the transport properties of the structure should be controlled by the motion of Josephson vortices rather than by the phase locking of spatially homogeneous interlayer junctions. It is also reasonable to note that superconducting transport measurements in the c direction are rather hard to perform, because single-crystal samples of these layered materials are often very thin and fragile. It is also difficult to control the cross-sectional area for current in the c direction. Moreover, with such crystals, it is not easy to limit and control the number of Cu-O layers, as is preferred in such experiments. Besides, there is always a risk of damaging the crystal along the fragile c plane during handling (it is known that $Bi_2Sr_2CaCu_2O_x$ cleaves very easily at Bi-O planes), making the crucial measurement unfeasible.

To make the situation more evident, we have performed a similar experiment using thin films where the samples were much more controllable and credible than the bulk ones. Unique high-quality "tilted" $Bi_2Sr_2CaCu_2O_x$ epitaxial films grown on tilted $SrTiO_3$ substrates[7] were employed for this purpose. The film Cu-O plane makes a finite angle with respect to the film plane, thus making a c-direction transport experiment possible and at the same time controllable. When prepared under the right conditions, the films can be made grain-boundary free and show respectable conduc-

tivity comparable with a good-quality single crystal in both the in-plane and out-of-plane directions. Utilizing such films, small-size interlayer "junctions" having about 200 interlayers (sometimes as few as 25 interlayers) were made.

II. FILMS

Epitaxial $Bi_2Sr_2CaCu_2O_x$ films grown on inclined $SrTiO_3$ substrates were used in this experiment. Details of the growth techniques and the epitaxial structures were described elsewhere.[7–9] Figure 1(b) shows a typical reflected high-energy electron-diffraction (RHEED) pattern toward $[\bar{1}\,\bar{1}0]$, and Fig. 1(a) shows the RHEED pattern toward $[1\bar{1}0]$. Clear streak patterns without additional spots as shown in Fig. 1(b) guarantee that the film has a very smooth surface and contains no precipitates. The fine streaks surrounding the central streak as seen in Fig. 1(a) appeared due to the incommensurate modulation along the b-axis direction. In addition to the existence of the incommensurate modulation streaks, the inclination of these streaks agrees with the substrate's tilt. It confirms that the film Cu-O planes have a certain angle with respect to the substrate surface, and the direction of the film was uniquely determined.

The inclination (typically 4°–12°) of the substrate surface toward [111] formed regular surface steps and terraces, and the epitaxy was restricted so as to tilt the c axis by the same angle from the substrate normal. Cross-sectional high-resolution transmission electron microscopy (TEM) (Fig. 2) revealed that the film contained relatively few defects, and the Bi-O planes ended at the film surface. The amount of the defects and intergrowths formed at the interface decreased rapidly with increasing distance from the substrate. The film can be made grain-boundary free up to tilt angles of 12°. Typical films had a T_c of about 35 K, and all the data used in this report had values between 33 and 40 K. The maximum J_c of about 3×10^6 A/cm^2 was obtained in the a-b plane at 4.2 K.

We observed a large resistive anisotropy between the a and b directions of the film. Patterned films were used for resistivity measurements with the four-probe method. A typical patterned shape is a 500-μm-long and 100-μm-wide rectangle. The in-plane resistivity $\rho_{[110]}$ along the step direction (4° inclined from [110] $SrTiO_3$) was about 20 times higher compared with ρ_a and showed a semiconductor temperature dependence. The resistivity along the a axis (ρ_a) showed a metallic temperature dependence.

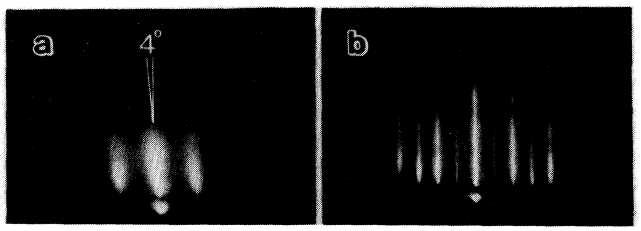

FIG. 1. RHEED patterns of a $Bi_2Sr_2CaCu_2O_x$ film grown on tilted substrates with electron beams in the $[1\bar{1}0]$ direction (a) and in $[\bar{1}\,\bar{1}0]$ direction (b).

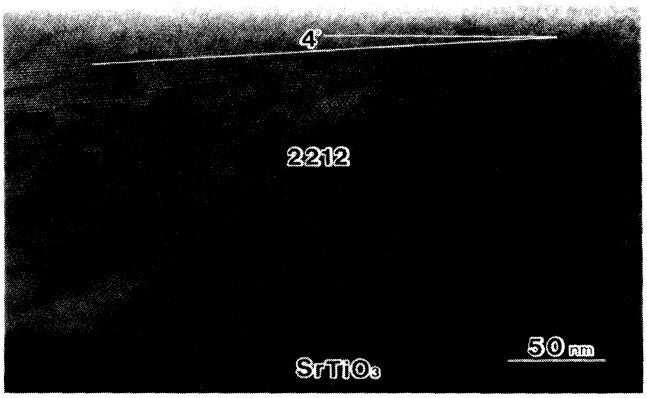

FIG. 2. TEM picture of the film cross section.

In analyzing the large in-plane anisotropy, we assume an ideal structure having perfect stacking of the half unit cell of the $Bi_2Sr_2CaCu_2O_x$ without intergrowth. Each half-unit-cell slab having 4° inclination toward [111] $SrTiO_3$ is terminated at the film surface as indicated from the TEM picture (Fig. 2). Hence the resistivity along the step direction involves a contribution from the c-axis component.

III. ANISOTROPY PARAMETER

To estimate ρ_c from the experimentally measured $\rho_{[110]}$ and ρ_a we start from the Laplace equation for the electric potential U:

$$\frac{\partial^2 U}{\partial x^2}+\frac{\partial^2 U}{\partial y^2}=0\ . \tag{1}$$

Taking into account the periodicity of the system (see Fig. 3)

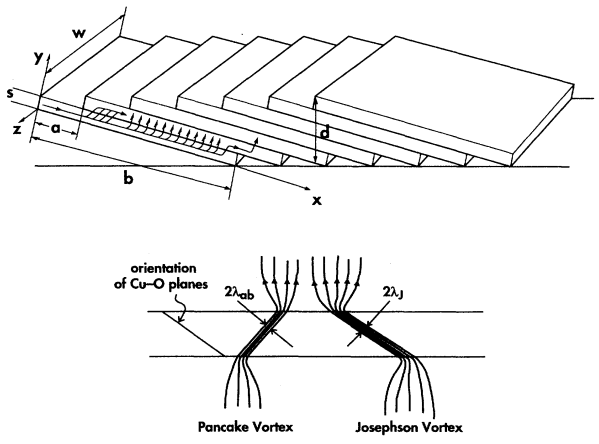

FIG. 3. (a) Schematic diagram of the sample. Each slab represents a unit cell. The arrows show the direction of current flow for C sample (current transverses the Cu-O/Cu-O interlayers). (b) Schematic view of the Josephson vortices and the pancake vortices in a sample (viewed sideways).

$$U(x,s\pm 0)=U(x-a,\pm 0)+U_0 , \quad (2)$$

we can reduce the solution of (1) to only one unit cell in the c direction. Here U_0 is a constant value. The boundary conditions for Eq. (1) at $x=0$ and $x=b$ are defined by the absence of current via the boundaries:

$$\frac{\partial}{\partial x}U(0,y)=0 , \quad \frac{\partial}{\partial x}U(b,y)=0 , \quad (3)$$

and the continuity of the current flow via the interfaces located at $y=0$ and $y=s$ gives

$$\gamma\lambda_J\frac{\partial}{\partial y}U(x,0)=-[U(x,+0)-U(x+a,s)+U_0] , \quad 0<x<(b-a) , \quad (4)$$

$$\gamma\lambda_J\frac{\partial}{\partial \gamma}U(x,s)=-[U(x-a,+0)-U(x,s)+U_0] , \quad 0<x<b , \quad (5)$$

$$\frac{\partial}{\partial y}U(x,0)=0 , \quad (b-a)<x<b , \quad (6)$$

$$\frac{\partial}{\partial y}U(x,s)=0 , \quad 0<x<a . \quad (7)$$

Here $\gamma=\sqrt{\rho_c/\rho_a}$ is the anisotropy parameter, and $\lambda_J=\gamma s$. In accordance with the structure, the following inequalities are assured:

$$s\ll a,\lambda_J , \quad a\ll\lambda_J . \quad (8)$$

The last inequality permits us to use the Taylor expansion for $U(x\pm a)$:

$$U(x+a,s)=U(x,s)+a\frac{\partial}{\partial x}U(x,s) , \quad U(x-a,0)=U(x,0)-a\frac{\partial}{\partial x}U(x,0) , \quad (9)$$

while the first inequality of (8) provides the possibilities to find the solution of (1) in the form of series on the small parameters (s/a), (s/λ_J), and (a/λ_J).

In the first approximation, we can neglect in (1) the derivation with respect to the coordinate x and find

$$U(x,y)=A(x)+B(x)\frac{y}{s} . \quad (10)$$

After the substitution of (10) into (1), in the second approximation we have

$$U(x,y)=A(x)+B(x)\frac{y}{s}\left[\frac{d^2A}{dx^2}\right]\frac{y^2}{2}-\left[\frac{d^2B}{dx^2}\right]\frac{y^3}{6s} . \quad (11)$$

The equation for the determination of the functions $A(x)$ and $B(x)$ directly follows from the boundary conditions (4)–(7). Taking into account the inequalities (8), it is easy to obtain

$$B(x)=s^2\frac{d^2A}{dx^2} , \quad \lambda_J^2\frac{d^2A}{dx^2}=-U_0 , \quad 0<x<a , \quad (12)$$

$$B(x)=-\frac{s^2}{\lambda_J^2}U_0 , \quad \frac{d^2A}{dx^2}=0 , \quad a<x<(b-a) , \quad (13)$$

$$B=0 , \quad \lambda_J^2\frac{d^2A}{dx^2}=U_0 , \quad (b-a)<x<b . \quad (14)$$

The solution of (12)–(14) with the boundary conditions (3) for the electric potential finally gives

$$U(x,y)=\frac{U_0}{2\lambda_J^2}\begin{cases}2a^2-b^2-x^2-2sy-y^2 , & 0<x<a,\\ 3a^2-b^2-2ax-2sy , & a<x<b-a,\\ x^2-2bx-y^2 , & b-a<x<b .\end{cases} \quad (15)$$

The current flowing via the structure is easily calculated as

$$I=-\frac{1}{\rho_a}\int_0^b\left[\frac{d}{dy}U(x,0)\right]dx=\frac{s(b-a)}{\rho_a\lambda_J^2}U_0=\frac{1}{\rho_{[110]}}U_0 \quad (16)$$

and after taking into account the geometry of the structure finally it leads to

$$\rho_{[110]}=\rho_c\frac{s}{d}\sin\theta\approx 10^{-3}\rho_c . \quad (17)$$

Here $s\sim 1.5$ nm is the distance between CuO layers, $d\approx 100$ nm is the film thickness, and $\theta\approx 4°$ and is the inclination angle. The observed value of $\rho_{[110]}$ was about 100 $\mu\Omega$ cm, giving $\rho_c\approx 1$ Ω cm.

From (17), for the anisotropy parameter and characteristic length λ_J of our films we have

$$\gamma=\sqrt{\rho_c/\rho_a}\approx 150 , \quad \lambda_J=\gamma s\approx 220 \text{ nm} . \quad (18)$$

These values are consistent with the data observed in bulk single crystals [$\gamma\approx 50$,[10] 500,[11] 300,[12] 100,[13] and 900 (Ref. 14)] and also near the value reported by Kleiner *et al.*[5] ($50<\gamma<280$). The large tolerance in the values of γ reported for single crystals can be understood if we take into account the influence of the oxygen content on the out-of-plane conductivity. Actually, band-structure calculations[15] for $Bi_2Sr_2CaCu_2O_x$ indicate that there are Bi-O bands crossing the Fermi level. This has to result in a metallic conductivity in the c direction and smaller γ. These calculations, however, do not take into account the incommensurate distortion of the Bi-O planes, which can bring the bands above the Fermi level[16] resulting in increased γ. Angle-resolved photoemission[17] and scanning tunneling spectroscopy[18] studies have shown that these planes could behave as either metallic or insulating, depending on the oxygen content, which in turn could depend on the conditions of synthesis of the crystal. In our samples, the resistivity $\rho_{[110]}$ increases rather weakly with decreasing temperature. It implies that, perhaps due to large oxygen content in our thin films, we have a better out-of-plane conductivity, and thus a smaller γ, compared to some of the bulk single crystals.[11,12,14]

IV. CURRENT-VOLTAGE CHARACTERISTICS

The films were delineated lithographically into small strips having dimensions of a few micrometers in width and length. As shown in the insets of Fig. 4, the orientation of the small strips was arranged in two ways. The

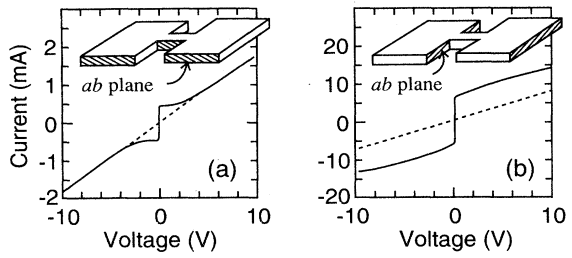

FIG. 4. I-V characteristics of a C sample (a), and an A sample (b). The orientation of the hatched lines on samples shown in the insets schematically indicates the arrangement of the Cu-O planes in the two types of sample.

hatched lines in these figures represent the orientation of the Cu-O planes. In one case, the current traverses the Cu-O/Cu-O interlayers (C sample); in the other case, the current flows parallel to the Cu-O basal planes (A sample). Figures 4(a) and 4(b) show I-V characteristics of both of these samples taken at 4.2 K. The striking difference in the I-V characteristics was fully reproducible for the 20 or so samples that we have tested.

All the C samples showed a resistively-shunted-junction (RSJ) "Josephson-like" characteristic similar to Fig. 4(a), having a rather rapid voltage increase just above a critical current I_c, and a resistance approaching a constant value R_n quickly without exhibiting any obvious "excess current" and giving a characteristic "upturned" curve. The I_cR_n products of these C samples were proportional to the number of the Cu-O/Cu-O interlayers in the strips, as shown in Fig. 5, where their low-temperature values are plotted. The shorter samples were influenced by an "end effect" that originates from the shallow tilting of the layers with respect to the film surfaces. The a-axis transport would influence the transport at two ends of a sample within the range of distance near L [see Fig. 3(a)]. Most of the samples were made using 4° films having a thickness of 0.05 μm. That would make L near 0.7 μm. In Fig. 5 we plotted the measurements on samples with lengths comfortably longer than the length L. Here, a 5-μm-long sample corresponds to about 230 layers. To calculate the I_cR_n value per interlayer in the c-axis direction, the conservation relation $I_cR_n/\text{layer}=j_c\rho_c s$ was used. Here, ρ_c is given by $\rho_c=\rho_{[110]}/\sin^2\theta$ when $\rho_{[110]}$ is obtained directly from R_n. This relation is different from Eq. (17) because shown $T<T_c\rho_a=0$ is assumed. The critical current density is given by $j_c=I_c/(b-a)w$, and this will be rigorously shown in Eq. (34) below. The current in a C sample had to flow through the tilted interlayers. Assuming its I-V characteristic was dominated by the interlayers, then the I_cR_n product of a C sample should simply represent the I_cR_n of the n interlayers in series [$n=(L\sin\theta)/s$], where the interlayer period $s=1.5$ nm and L is the strip length. Figure 5 shows that the I_cR_n per interlayer was about 9 mV at $T=4.2$ K. This value is close to that expected from the Ambegaokar and Baratoff formalism for an ideal junction, which gives $I_cR_n=\pi\Delta(0)/2e$ at low temperature.

All the A samples showed "flux-flow-like" characteristics similar to the one shown in Fig. 4(b), where the resistance above I_c does not approach a linear resistance R_n even at voltages considerably above I_cR_n, giving a finite amount of "excess current." Such behavior is consistent with other experiments showing that flux motion dominates the dissipation during ab-plane transport.[19]

Figure 6 shows the temperature dependence of I_cR_n products along the c axis and the a axis, normalized by the relevant lengths l^*($l^*=L\sin\theta$ for C samples and $l^*=L$ for A samples). It is difficult to define the resistance R_n for A samples. However, in order to demonstrate the difference in I_cR_n in the two transport directions, here we picked the value around 10 V. Critical current densities J_c along the a axis and the c axis for the corresponding samples are also plotted on a logarithmic scale.

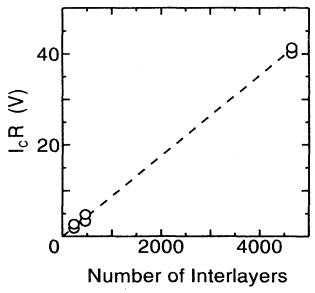

FIG. 5. Relationship between I_cR_n product of C samples and the number of interlayers contained in the corresponding samples.

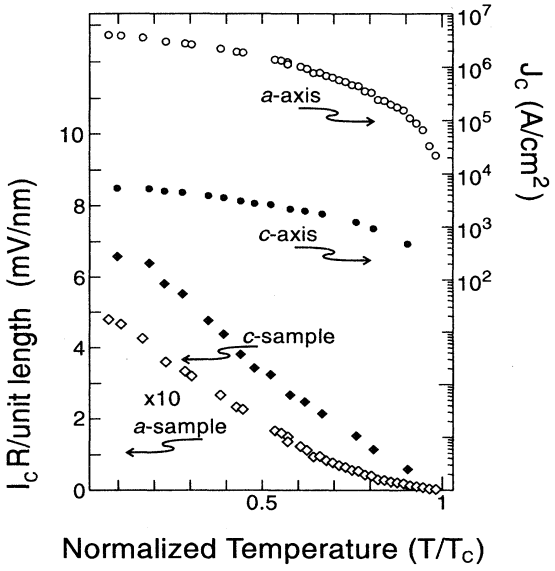

FIG. 6. Temperature dependencies of I_cR_n and J_c.

V. TEST OF JOSEPHSON EFFECT

The reproducible differences in I-V characteristics, critical current densities, and I_cR_n along the two transport directions provided us with evidence of strong transport anisotropy. Furthermore, the shape of the I-V characteristics, as well as the value of I_cR_n per interlayer, perhaps suggest it is a direct observation of the interlayer Josephson effect. Nevertheless, the most obvious signatures of a Josephson junction are ac and dc Josephson effects. We have carried out experiments with external microwave irradiation and applied magnetic fields to verify these quantum effects.

Figure 7 shows the I-V characteristic of a C sample and an A sample with applied microwave radiation, taken at elevated temperatures. Higher temperatures were used to reduce I_c and I_cR_n, so that applied microwaves could sufficiently reduce the critical currents, at the same time reducing the characteristic frequency to match the applied microwave frequency. From Fig. 7(a), taking the value of R_n from the microwave-suppressed resistance, I_cR_n at this temperature was about 14 mV, which corresponds to about 70 μV/layer. Both Figs. 7(a) and 7(b) show a similar modulation: critical currents were suppressed to zero, and some unknown nonlinearity with a "kink" appeared, but there were no ac Josephson voltage steps in either sample. None of the samples tested showed any sign of the appearance of quantized voltage steps. For some samples, in order to improve the voltage matching between the Josephson voltage $\Phi_0 v$ and characteristic voltage I_cR_n, extra shunt resistance was provided by evaporating thin *in situ* gold films on top of these samples, making the equivalent I_cR_n per layer near 10 μV, which corresponds to a characteristic frequency of 5 GHz. But Josephson steps were not observed in the shunted samples either.

Figures 8(a) and 8(b) show the external magnetic-field dependence of the critical current for a C sample, with two applied-field scanning directions, taken at 4.2 K. The schematics in Fig. 8 define relationship of the current and field. The field was scanned at two angles, ζ and ϕ. The insets in Fig. 8 show the field dependence on I_c in a larger field scale up to 7 T. In Fig. 8(a), when the applied field was in the direction $\phi_0=0°$, the would-be-expected periodic of I_c modulation is $B=\Phi_0$, where Φ_0 is the flux quantum, s is the interlayer period 1.5 nm, $d=150$ nm, and $\theta=4°$. For Fig. 8(b), the corresponding period for $\zeta=0°$ is $B=\Phi_0/sw\approx 0.2$ T, with the width of the strip $w=6$ nm. In both Figs. 8(a) and 8(b), no apparent I_c modulation period was observed.

The angular dependence of the critical currents in the ζ scan and the ϕ scan of the same sample used in Fig. 8 showed the maximum critical current suppression at $\zeta\approx 90°$ and $\phi\approx 90°$. No suppression was seen for $\zeta=0°$ and $\phi\approx 0°$.

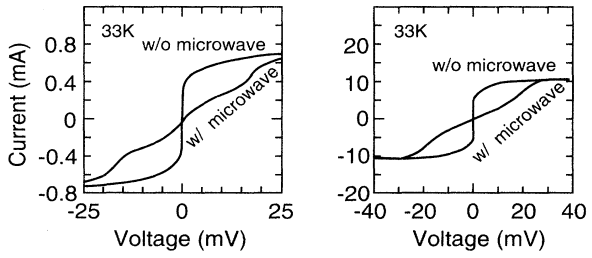

FIG. 7. I-V characteristics of a C sample (a) and an A sample (b) with and without microwave irradiation [1.5 GHz for (a) and 0.5 GHz for (b)]. Data were taken at temperatures closer to T_c in order to reduce I_cR_n. Josephson voltage steps were not observed under all the conditions tried, even when I_c was suppressed to zero.

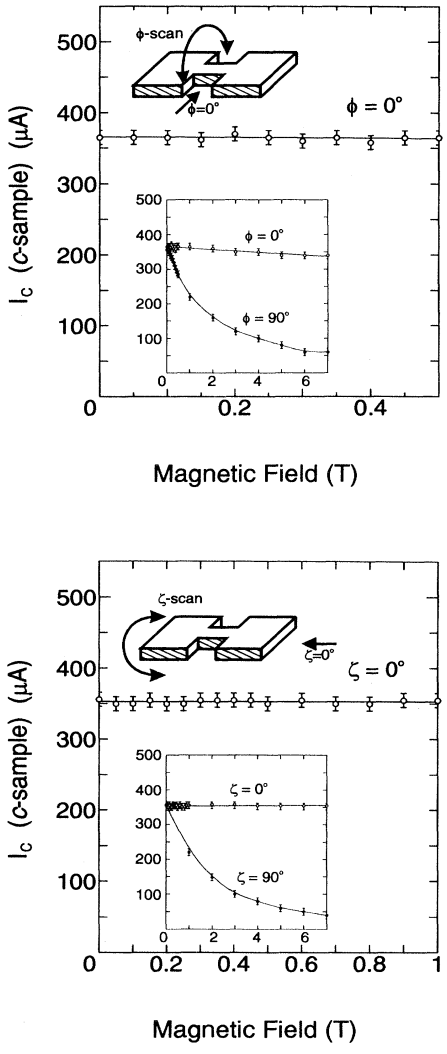

FIG. 8. Magnetic-field dependencies for I_c under ϕ scan (a) and ζ scan (b) for a C sample. The directions of the magnetic fields are shown in the insets. The orientation of the hatched lines shown in the insets schematically indicates the arrangement of the Cu-O planes in the sample. The low insets show the fields dependencies up to 7 T. I_c should be modulated with periods 0.6 T ($\phi=0$) or 0.2 T ($\zeta=0$) if it was characterized by Josephson coupling.

VI. DISCUSSION

The observed phenomena are in contrast to those reported by Kleiner *et al.*[5] despite the practically identical material constants of $Bi_2Sr_2CaCu_2O_x$, and the even smaller geometrical dimensions in our samples.

To understand the reasons for this difference in the results, it is necessary to check the conditions that guarantee the observation of Shapiro steps and the Fraunhofer pattern. It is well known that for junctions with bulk superconductive electrodes, in order to see these effects, it is required to have a homogeneous distribution of supercurrent in the junction region. It is satisfied if the junction's width w is smaller than the Josephson penetration depth λ_c. In our samples this restriction is satisfied, since

$$w \approx 5\ \mu\text{m} \ll \lambda_c = \gamma \lambda_a = 28\ \mu m\ . \tag{19}$$

For a stacked junction configuration with a small thickness of electrodes s compare to λ_a the situation is drastically change due to the existence of two characteristic lengths λ_c and λ_J responsible for the behavior of the system.[4,20] In Ref. 20 it was shown that the gauge-invariant phase difference of the order parameter of the neighboring stacked layers $\varphi_{n,n+1}$ must satisfy the equations

$$\nabla^2 \varphi_{n,n+1} - \frac{1}{\lambda_J^2}(2\sin\varphi_{n,n+1} - \sin\varphi_{n+1,n+2} - \sin\varphi_{n-1,n}) - \frac{1}{\lambda_c^2}\sin\varphi_{n,n+1} = 0\ , \tag{20}$$

$$\nabla_x \varphi_{n,n+1}(x=0,b) = \frac{2\pi s}{\Phi_0} H\ , \tag{21}$$

$$j_z = \frac{c\Phi_0}{8\pi^2 \lambda_c^2 s}\sin\varphi_{n,n+1}\ . \tag{22}$$

Here ∇ is the differential operator in x,y plane (see Fig. 3) and $H=(0,0,H)$ is the external magnetic field. From (20)–(22) it follows that in the limit

$$b \ll \lambda_c \tag{23}$$

the Meissner state in the sample an be described by a solution

$$\varphi_{n,n+1} = \frac{2\pi s x}{\Phi_0} H + \arcsin\frac{j}{j_0}\ ,\quad j_0 = \frac{c\Phi_0}{8\pi^2\lambda_c^2 s}\ , \tag{24}$$

where j is the density of the bias current, which is independent of the coordinates (x,y). However, the Meissner state in the system is unstable against the formation of a static mixed state due to penetration of the vortices in the sample, because of the small size of the Josephson vortices λ_J [Eq. (18)] compared to the size of the electrodes b.[21] That means that the restriction (23) alone cannot guarantee the observation of the classical behavior of Josephson junctions.

The transition between stationary and flux-flow regimes in the mixed sate takes place at a current density lower than the critical current density j_0. So to check the existence of the Meissner state in our samples it is necessary to compare the experimental value j_c with the theoretical one, taking into account the possible deviations from homogeneity due to the specific geometry of the film.

To calculate j_c at zero magnetic field we introduce the gauge-invariant phase of the order parameter of the separate layer χ, which under restriction (23) satisfies the equation

$$\frac{\partial^2\chi}{\partial x^2} + \frac{\partial^2\chi}{\partial y^2} = 0 \tag{25}$$

with the boundary conditions at the interfaces (see Fig. 3)

$$\frac{\partial}{\partial x}\chi(0,y) = 0\ ,\quad \frac{\partial}{\partial x}\chi(b,y) = 0\ , \tag{26}$$

$$\frac{\partial}{\partial y}\chi(x,s) = 0\ ,\quad 0 < x < a\ , \tag{27}$$

$$\frac{\partial}{\partial y}\chi(x,s) = \frac{1}{\gamma\lambda_J}\sin[\chi(x,s+0) - \chi(x,s-0)]\ ,\quad a < x < b\ , \tag{28}$$

$$\frac{\partial}{\partial y}\chi(x,0) = \frac{1}{\gamma\lambda_J}\sin[\chi(x,+0) - \chi(x,-0)]\ ,\quad a < x < b-a\ , \tag{29}$$

$$\frac{\partial}{\partial y}\chi(x,0) = 0\ ,\quad b-a < x < b\ . \tag{30}$$

Equations (28) and (29) follow from the continuity of the supercurrent via interfaces, while (26), (27), and (30) guarantee the absence of the current via the free boundary.

The solution of Eqs. (25)–(30) can be found in the same manner as we have done in calculating the film resistivity in Sec. III. Taking advantage of the periodicity of the system, we can introduce the constant phase difference between the layers by the relationships

$$\chi(x,s\pm 0) = \chi(x-a,\pm 0) + \varphi_0 \tag{31}$$

and reduce the problem to the solution of the equation in a single layer. The inequalities (8) provide the possibility to find this solution in the form of series on the parameters s/a, s/λ_J, and a/λ_J and we finally obtain

$$\chi = \frac{\sin\varphi_0}{\lambda_J^2} \times \begin{cases} 2ab - b^2 + sy - (x^2+y^2)/2\ , & 0 < x < a, \\ (b-a)^2/2 - ax + sy\ , & a < x < b-a, \\ bx + (y^2 - x^2)/2\ , & b-a < x < b\ . \end{cases} \tag{32}$$

The value of the total current flowing through the film can be calculated by the integration

$$I = \int_0^b \left[-\frac{c\Phi_0}{8\pi^2\lambda_a^2}\frac{\partial}{\partial y}\chi(x,0) \right] dx = \frac{c\Phi_0(b-a)}{8\pi^2\lambda_c^2 s}\sin\varphi_0\ , \tag{33}$$

resulting in

$$j_c = \frac{I_c}{(b-a)w} = j_0\ . \tag{34}$$

The difference between theoretical ($j_0 \approx 2.2\times10^4$ A/cm^2) and experimental [$j_c = I_c/(b-a)w \approx 8\times10^3$ A/cm for $w = 5$ μm] values of critical current density at $T = 4.2$ K reveals that it is the mixed state in the film that is responsible for the critical current value.

For a C sample, at zero external magnetic field we can expect the formation of two kinds of mixed states. As follows from (32), in the interior part of the film supercurrent flows basically in the y direction, generating a component of the magnetic field parallel to the layers. This component results in the formation of mixed state due to penetration of the Josephson vortices in the sample between the Cu-O layers [see Fig. 3(b)]. The structure of these vortices is closer to the Abrikosov ones rather than to the usual Josephson ones.[21] The existence of two characteristic lengths in (20), as in the Abrikosov case, results in the formation of a core region with a radius of the order of λ_J. But in contrast to the Abrikosov vortices there is no suppression of the order parameter in the Cu-O planes in this core region. It corresponds to the area where supercurrent increases with the distance l from the vortex center, achieving the maximum critical current density at $l \approx l_0 \approx 0.5\lambda_J$. At $l > l_0$ the supercurrent density falls exponentially with decay lengths λ_c and λ_J in the plane (x) and perpendicular to the plane (y) directions, respectively.

From (32) it follows that tin our tilted C samples we also have a current along the Cu-O layers:

$$j_x = \frac{c\Phi_0 a}{8\pi^2\lambda_a^2\lambda_J^2} = \frac{c\Phi_0 a}{8\pi^2\lambda_c^2 s^2} \approx \frac{a}{s} j_y \tag{35}$$

with a current density approximately 10 times larger than in the direction perpendicular to the Cu-O plane. It generates a component of the magnetic field perpendicular to the superconducting planes, resulting in the formation of a mixed state with vortices in the characteristic pancake structure.[23] In this case the I_c value is defined by the transition so the system into a dynamic mixed state of the pancake.

For an A sample, the current distribution only allows the formation of the pancake vortices. The different shapes of the I-V characteristics systematically observed for A and C samples can be understood as the result of the motion of the two types of vortices. For A samples, the I-V curve [Fig. 4(a)] is quite similar to that obtained from most other superconducting films under pancake-vortex flow. For C samples, however, the existence of the Josephson vortices results in the generation of other types of flux flow. It has been predicted that, under a periodic and harmonic pinning potential, the stable and synchronous motion of the vortices would produce an RSJ-like I-V characteristic taking the expression[22]

$$V = R_n(I^2 - I_c^2)^{\alpha}, \quad \alpha = \tfrac{1}{2}. \tag{36}$$

The critical current density of the C sample is much smaller than that of A sample, indicating a weaker effective pinning force in these samples. From the observed I-V characteristic of the C samples, we found it could be fitted to expression (36) rather well with the power $\alpha \cong 0.4$–0.8 (Fig. 9), agreeing with the prediction.

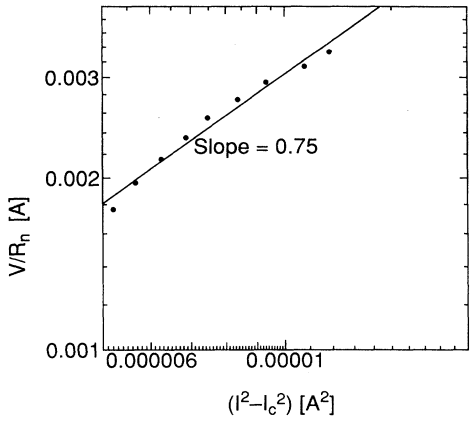

FIG. 9. Power-law fitting of I-V characteristics of a C sample. It shows it can be expressed in a form $V = R_n(I^2 - I_c^2)^{\alpha}$ with $\alpha \sim 0.75$ for this particular sample.

We believe the voltage-generating mechanism in C samples is the motion of the Josephson vortices, not that of the pancake vortices. This is because in the usual c-axis film, which only contains pancake vortices, such an "upturned" ($a < 1$) I-V characteristic has never been reported. In addition, this could be an observation of such I-V characteristics obtained from a flux-flow system.

The absence of the ac and dc Josephson effects can also be explained by this model, for critical currents in these junctions are not restricted by the Josephson effect, but by the flux flow. The motions of these large number of vortices are impossible to be synchronized by the external microwave irradiation. The observed field dependence of the I_c in magnetic fields perpendicular to the C-sample surface ($\phi = 90°$ and $\zeta = 90°$ of Fig. 8) are very similar to that of the typical c-oriented temperature superconductor (HTS) films, confirming the vortex-flow picture. For a stack of small thickness $d < \lambda_a$, which is close to our case, the magnetic-field component with $\phi = 0°$ and $\zeta = 0°$ cannot be screened by the superconductor. The magnetic field parallel to the plane is distributed homogeneously in the film, both in the superconducting Cu-O planes and in the interlayer junctions, and does not affect the critical current value due to the absence of the Meissner effect. This directly follows from the measured dependencies of $I_c(H)$, which confirm that for both ϕ and ζ scans there is practically no influence of the external magnetic field on I_c at $\phi = 0°$ and $\zeta = 0°$, respectively. So we can conclude that it is not the Josephson coupling as in the spatially homogeneous junction that is responsible for the critical current value.

VII. CONCLUSIONS

a- and c-axis transport measurements with well-controlled junction geometry were performed on tilted $Bi_2Sr_2CaCu_2O_x$ thin films. The quality of the films was rather good, having an anisotropy parameter of $\gamma = \sqrt{\rho_c/\rho_a} \approx 150$, and without showing any obvious formation of intergrowth or other crystals phases. The

scope of the observed data reveals that the voltage-generating mechanism in both configurations is due to the motion of vortices (pancake vortices for the A samples; Josephson vortices for the C samples), not the Josephson effect. It reduces the critical current density by many orders of magnitude below the theoretical value j_0. The field dependence of the critical current in Fig. 8, with $\phi=90°$ and $\zeta=90°$, also supports such a mechanism. Perhaps this is reasonable considering the fact that the specific geometry of our samples is larger than the Josephson penetration depth of the material. The constraints in the sample geometry,

$$w,b \ll \lambda_J \ , \tag{37}$$

should be satisfied, in order not to introduce Josephson vortices into the sample. Compared to our experiment, the experiment described in Ref. 5 had an even smaller j_c and larger geometrical junction size. In the light of our experimental results and analysis, a consistent demonstration of the interlayer Josephson effect in these materials should be, and is yet to be, performed in a more convincing and more systematic manner.

The second important point inferred from the experimental data is the observed independence of the critical current upon the magnetic field parallel to the layer. It means that under the condition of Eq. (37), which guaranteed the absence of the mixed state of Josephson vortices in the stack,[4] the conditions, which lead to the absence of magnetic-field screening by the superconducting CuO planes,

$$w,b \leq \lambda_a \ , \tag{38}$$

should be satisfied simultaneously, since $\lambda_a \approx \lambda_J$ in the Bi-based material. That means that if we succeeded in fabricating this type of structure we would realize a unique Josephson element whose proprieties are not influenced by the external magnetic-field environment. The possibility of fabricating this type of structure is quite high even with present-day technology, because of the rather large London penetration depth at zero temperature for HTS materials from 140 to 350 nm.[24–32] Fabrication of such magnetically independent Josephson junctions is in progress now.

ACKNOWLEDGMENTS

This work was performed, in part, under the management of R&D Association for Future Electron Devices as a pat of the R&D of Basic Technology for Future Industries Supported by New Energy and Industrial Technology Development Organization.

*Permanent address: Institute of Nuclear Physics, Moscow State University, 119899 GSP Moscow, Russia.

[1]T. K. Worthington, W. J. Gallagher, and T. R. Dinger, Phys. Rev. Lett. **59**, 1160 (1992).

[2]G. Briceno, M. F. Crammie, and A. Zettl, Phys. Rev. Lett. **66**, 2164 (1991).

[3]Y. Koike, T. Nakamyo, and T. Fukase, Jpn. J. Appl. Phys. **27**, L841 (1988).

[4]B. A. Aminov, A. A. Bush, L. I. Leonyuk, T. E. Oskina, M. V. Pedyash, D. K. Petrov, Ya. G. Ponomarev, H. T. Rakhimov, K. Sethupathi, and M. V. Sudakova, in *Superconductor Devices and Application,* Proceedings of the 4th International Conference SQUID-91, Berlin, 1991, edited by H. Koch and H. Lubbig (Springer-Verlag, Berlin, 1992), pp. 45–48; Fiz. Nizk. Temp. Kiev) **17**, 692 (1991) [Sov. J. Low Temp. Phys. **17**, 364 (1991)].

[5]R. Kleiner, F. Steinmeyer, G. Kunkel, and P. Muller, Phys. Rev. Lett. **68**, 2394 (1992); R. Kleiner, and P. Muller, Phys. Rev. B **49**, 1327 (1994).

[6]L. N. Bulaevskii, J. R. Clem, and L. I. Glazman, Phys. Rev. B **46**, 350 (1992).

[7]J. Fujita, T. Yoshitake, T. Satoh, and H. Igarashi, Appl. Phys. Lett. **59**, 2445 (1991).

[8]J. Fujita, T. Yoshitake, T. Satoh, and H. Igarashi, IEEE Trans. Mag. **27**, 1205 (1991).

[9]T. Satoh, J. Fujita, T. Yoshitake, and H. Igarashi, Physica C **191**, 359 (1992).

[10]O. Laborde, P. Monceau, M. Potel, P. Gougeon, J. Padiou, J. C. Levet, and A. Noel, Solid State Commun. **67**, 609 (1988).

[11]J. R. Cooper, L. Forro, and B. Keszei, Nature **343**, 444 (1990).

[12]S. Martin *et al.*, Appl. Phys. Lett. **54**, 72 (1989).

[13]G. Briceno, M. F. Crommie, and A. Zettl, Phys. Rev. Let. **66**, 2164 (1991).

[14]F. X. Regi *et al.*, IEEE Trans. Appl. Supercond. **3**, 1051 (1993).

[15]H. Krakauer and W. E. Pickett, Phys. Rev. Lett. **60**, 1665 (1988).

[16]J. Ren, *et al.*, Physica C **158**, 501 (1989).

[17]B. O. Wells *et al.*, Phys. Rev. Lett. **65**, 3056 (1990).

[18]S. B. Samanta, P. K. Dutat, V. P. S. Awana, and A. V. Narlikar, Europhys. Lett. **16**, 391 (1991).

[19]Y. Iye, T. Tamegai, and S. Nakamura, Physica C **174**, 227 (1991).

[20]L. Bulaevskii and J. R. Clem, Phys. Rev. B **44**, 10 234 (1991).

[21]J. R. Clem and M. J. Coffey, Phys. Rev. B **42**, 6209 (1990).

[22]J. E. Evetts and J. R. Appleyard, in *Proceedings of the International Discussion Meeting on Flux Pinning in Superconductors, Sonnenberg, Germany, 1974,* edited by P. Haasen, and C. Freyhardt (Akademii der Wissenschften, Göttingen, 1974), p. 73; see also A. I. Larkin and Yu. N. Ovchinnikov, Sov. Phys. JETP **53**, 1221 (1981).

[23]J. R. Clem, Phys. Rev. B **43**, 7837 (1991).

[24]P. Birrier *et al.*, Physica C **158**, 230 (1989).

[25]A. Schilling, F. Hulliger, and H. R. Ott, Z. Phys. B **82**, 9 (1991).

[26]S. Mitra *et al.*, Phys. Rev. B **40**, 2674 (1989).

[27]S. Gygax, X. Xing, O. Rajora, and A. Curzon, Physica C **162–164**, 1551 (1989).

[28]M. Daumling and G. V. Chandrashekhar, Phys. Rev. B **46**, 6422 (1992).

[29]J. R. Thompson, D. K. Christen, H. A. Deeds, Y. C. Kim, J. Brynestat, S. T. Sekula, and J. Budai, Phys. Rev. B **41**, 7293 (1990).

[30]D. R. Harshamn, L. F. Schneemeyer, J. V. Waszczak, G. Aeppli, R. J. Cava, B. Batlogg, and L. W. Rupp, Phys. Rev. B **39**, 851 (1989).

[31]L. Krusin-Elbaum, R. L. Greene, F. Holtzberg, A. P. Malozemoff, and Y. Yeshurun, Phys. Rev. Lett. **62**, 217 (1989).

[32]A. Schilling, F. Hulliger, and H. R. Ott, Physica C **168**, 272 (1990).

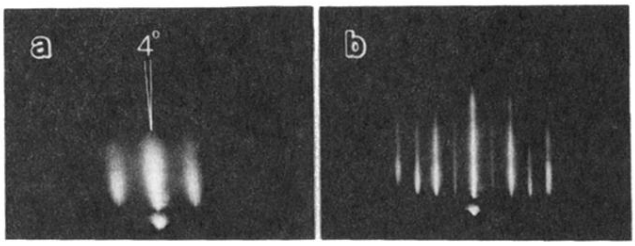

FIG. 1. RHEED patterns of a $Bi_2Sr_2CaCu_2O_x$ film grown on tilted substrates with electron beams in the $[1\bar{1}0]$ direction (a) and in $[\bar{1}\,\bar{1}0]$ direction (b).

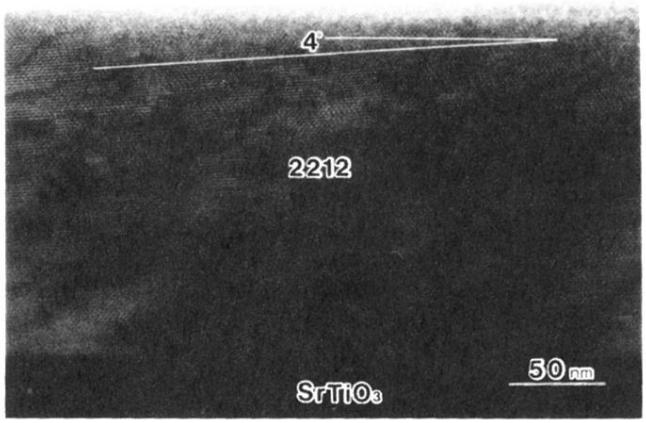

FIG. 2. TEM picture of the film cross section.